Hindawi
Shock and Vibration
Volume 2019, Article ID 8479395, 11 pages
https://doi.org/10.1155/2019/8479395

Research Article

Estimation of the Defect Width on the Outer Race of a Rolling Element Bearing under Time-Varying Speed Conditions

Guang-Quan Hou[1] **and Chang-Myung Lee**[1,2]

[1]*Department of Mechanical and Automotive Engineering, University of Ulsan, 93 Daehak-ro, Nam-Gu, Ulsan 44610, Republic of Korea*
[2]*Lavrentyev Institute of Hydrodynamics, Siberian Brunch of Russian Academy of Sciences, 15 Lavrentyev Ave., Novosibirsk 630090, Russia*

Correspondence should be addressed to Chang-Myung Lee; cmlee@ulsan.ac.kr

Received 21 June 2018; Accepted 6 November 2018; Published 3 January 2019

Academic Editor: Lutz Auersch

Fault diagnosis and failure prognostics for rolling element bearing are helpful for preventing equipment failure and predicting the remaining useful life (RUL) to avoid catastrophic failure. Spall size is an important fault feature for RUL prediction, and most research work has focused on estimating the fault size under constant speed conditions. However, estimation of the defect width under time-varying speed conditions is still a challenge. In this paper, a method is proposed to solve this problem. To enhance the entry and exit events, the edited cepstrum is used to remove the determined components. The preprocessed signal is resampled from the time domain to the angular domain to eliminate the effect of speed variation and measure the defect size of a rolling element bearing on outer race. Next, the transient impulse components are extracted by local mean decomposition. The entry and exit points when the roller passes over the defect width on the outer race were identified by further processing the extracted signal with time-frequency analysis based on the continuous wavelet transform. The defect size can be calculated with the angle duration, which is measured from the identified entry and exit points. The proposed method was validated experimentally.

1. Introduction

Rolling element bearings are one of the critical components in rotating machines, where faults such as the spalling and the pitting are commonly observed in the course of normal operation [1]. Therefore, the diagnosis of rotating machinery faults and failure prognostics is necessary to prevent equipment failure or predict the remaining useful life (RUL) to avoid catastrophic failure. The spall size is very small in the early stages of the fault and gradually deteriorated until the bearing breaks. Therefore, spall size can be used as a good fault feature for RUL prediction. However, fault size estimation for rolling element bearings can be a challenging task due to the harsh and variable working conditions.

To estimate the defect size of rolling element bearings, kinds of signal processing methods have been proposed. Epps [2] identified two events caused by a bearing fault: the point of entry and the point of impact. The defect size of a bearing was estimated by the time to impact (TTI). Sawalhi and Randall [3] illustrated more detailed explanation of the two events by observing the vibration signatures of seeded faults. To improve the estimation performance, Sawalhi et al. [4] and Ismail and Sawalhi [5] proposed other methods to process the vibration signal, such as autoregressive inverse filtration, synchronous averaging, energy envelopes, and numerical differentiation.

Other signal processing methods have also been proposed to measure the defect size of a bearing under different conditions. Jena and Panigrahi [6] measured different defect sizes in the inner and outer race of a bearing under constant speed. The ridge spectrum was derived from the continuous wavelet transform (CWT) to obtain an obvious indication of the time duration between the entry point and the exit point. Moustafa et al. [7] estimated the different seeded fault widths under low speed with an instantaneous angular speed (IAS) technique. The IAS could effectively reveal the shaft speed variation of a

bearing with a fault in the outer race when the rolling element passed through the defect area. Khanam et al. [8] detected different fault sizes in the outer race of a ball bearing by using the discrete wavelet transform analysis. The entry and exit events were pointed out clearly in the decomposed signal, and a good estimation of the defect size was obtained. Wang et al. [9] proposed a vibration signal processing methodology for extracting the fault size of a naturally generated fault and observing the propagation of a bearing fault under high-speed conditions. The entry and exit events in the vibration signal were enhanced by tacholess synchronous signal averaging (SSA) and the wavelet transform.

Previous research has focused on estimating the defect size of bearings under constant speed conditions. The signal enhancement processing methods have been applied based on the assumption of constant speed conditions [10]. However, rotating machinery sometimes works under time-varying speed conditions. In such conditions, the amplitude and fault characteristic frequency (FCF) of the rolling element bearing vibration signal are influenced by the time-varying speed [11]. Hence, envelope analysis and other enhancement techniques based on constant speed conditions cannot be applied directly.

Techniques have been proposed to process nonstationary vibration signals [1, 12–15]. Order tracking (OT) is widely used among those techniques, which can eliminate the effect of speed fluctuation [16]. The main idea of OT is to transform the time-varying speed vibration signal in the time domain to the angular domain with constant angle interval sampling. Thus, the effect caused by the time-varying speed is removed by resampling the signal into the angular domain. Provided that the defect width is constant, the shaft rotating angle is constant when the roller passes the defect width. Therefore, the defect width can be calculated from the resampled signal.

Although OT can eliminate the effect of speed fluctuation, it is still difficult to estimate the defect size of the bearing on the outer race because the impulse component of the signal is smeared by the noise signal. To extract the impact component of the signal, signal processing techniques can be used to extract fault information, such as wavelet transform (WT), empirical mode decomposition (EMD), and local mean decomposition (LMD) for a nonstationary signal. LMD is a novel signal processing method that was proposed by Smith [17]. It is an adaptive time-frequency signal processing method and has been successfully used for bearing fault diagnosis and has similar properties to EMD. In contrast to EMD, the LMD method uses the moving average to obtain the amplitude envelope instead of cubic spline interpolation. The overshooting and undershooting effect caused by cubic interpolation can be eliminated [18]. A series of product functions (PFs) can be obtained by the LMD processing method, and each PF represents a monocomponent of the original signal, which contains multiple components. Thus, LMD method is used in this study to extract the impact component from the multicomponent signal.

Energy is lost when a roller enters the leading edge of a defect, and high energy is generated when a roller hits the ending edge of the defect. Considering this, the position of the entry and exit points can be identified with time-frequency analysis, which can represent the energy distribution of the vibration signal. To obtain the exact position of the entry and exit points, the continuous wavelet transform can be used based on the characteristics of high time-frequency resolution [19]. The Morlet wavelet has been widely used to diagnose rolling bearing faults because its shape characteristic is similar to the impulse component of a rolling bearing signal [20]. To obtain the optimal wavelet that matches the vibration signal, it is very important to select appropriate parameters for the Morlet wavelet (the bandwidth and center frequency). Researchers have proposed methods to optimize the bandwidth and center frequency [21–23]. Once the optimized bandwidth and center frequency are obtained, the denoised signal can be processed with the CWT based on the Morlet wavelet.

In this paper, a new signal processing scheme is proposed to detect the fault size of a rolling element bearing under time-varying speed conditions. The whole procedure of the proposed method is shown in Figure 1. To enhance the entry and exit events, the edited cepstrum technique is used to remove the determined component of the signal, and the preprocessed signal is resampled by constant angle interval sampling with a tachometer signal to eliminate the effect of speed variation and measure the defect width. The impact component of the fault bearing signal is obtained with the LMD method for further time-frequency analysis. The extracted component is then processed using the CWT, for which the Morlet wavelet is selected as the mother wavelet. The entry and exit points, when the roller passes over the defect on the outer race, can be identified from the scalogram. The defect width is calculated with the angle duration, which is measured from the identified entry and exit points. The proposed method was verified experimentally.

2. Signal Preprocessing

2.1. Cepstrum Prewhitening. A bearing fault signal based on time-varying speed conditions consists of an impulse fault component, determined component, and random noise component. The cepstrum is the inverse Fourier transform of the log spectrum [23, 24]. The main purpose of using the cepstrum prewhitening (CPW) technique is to separate the determined component from the vibration signal [24, 25]. Once the constant component signal has been removed, the entry and exit events are enhanced. For a given vibration signal $x(t)$, the cepstrum is defined as follows:

$$C(q) = F^{-1}\{\ln(A(f)) + j\varphi(f)\}, \tag{1}$$

where q is the quefrency and $X(f)$ is the Fourier transform of $x(t)$:

$$X(f) = F\{x(t)\} = A(f)e^{j\varphi(f)}. \tag{2}$$

The real cepstrum can be obtained by the real part in equation (1).

Cepstrum analysis can concentrate the harmonic components into a series of peaks. The cepstrum peaks in the quefrency domain indicate periodic harmonic components

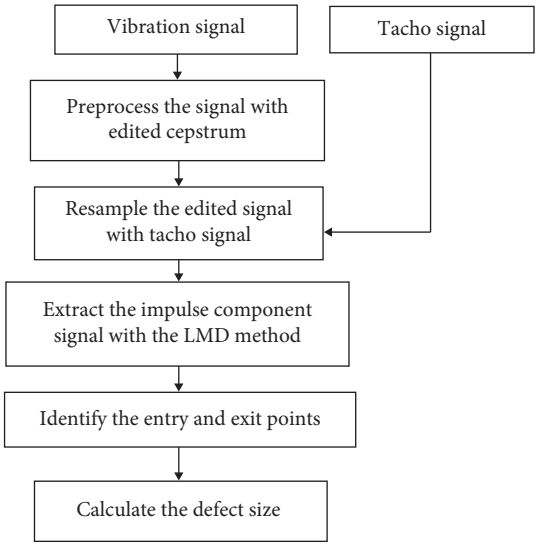

Figure 1: Flow chart of the fault size estimation approach.

in the spectrum. It is a simple way to separate to deterministic components from the vibration signal by editing the amplitude of the real cepstrum. The cepstrum editing procedure is shown in Figure 2. There are two ways to edit the real cepstrum signal. The first one is setting a zero value for the whole real cepstrum (except possibly at zero quefrency), so that the discrete harmonics and resonances are eliminated in the frequency domain. The prewhitened signal can be obtained by recombining the edited cepstrum signal with the phase information of the original signal and inverse transforming to the time domain. The other one is eliminating the deterministic excitations by removing the peaks with filtering operations, which is a cepstrum editing procedure. The edited cepstrum signal is then transformed to the frequency domain. The edited real cepstrum signal can be obtained by recombining the edited cepstrum signal with the phase information of the original signal and inverse transforming to time domain.

The cepstrum editing method was used to remove the constant components from the signal. By using the CPW technique, the entry and exit events of rolling elements passing the defect area were enhanced. However, it is still hard to determine the obvious entry and exit points in the time domain due to the effect of random noise and speed variation. To identify the entry and exit points, other techniques are used to analyze the nonstationary signal.

2.2. Resampling Method. When the entry and exit points are identified, the duration of the rollers rolling over a defect is obtained. The fault size can then be estimated by the following equation (assuming the contact angle is zero):

$$L_{\text{defect}} = \frac{\pi T_{\text{impact}} f_{\text{shaft}} \left(D_{\text{p}}^2 - D_{\text{roller}}^2\right)}{D_{\text{p}} f_{\text{s}}}, \tag{3}$$

where f_{shaft} is the speed of shaft, f_{s} is the sampling rate, T_{impact} is the time to impact, D_{roller} is the roller diameter, and D_{p} is the pitch diameter. However, for the time-varying speed conditions, the equation is not suitable because the shaft speed varies. If the angle of the shaft when passing the defect is known, the defect size can be calculated with the geometric parameters of the rolling bearing. Therefore, to measure the defect size under time-varying conditions, the signal needs to be resampled from the time domain to the angular domain.

The conventional resampling method uses a constant angle interval instead of a constant time interval. In the resampling procedure, the speed information is obtained by a tachometer. The main steps of the resampling process include the following [13, 26, 27]:

(1) Synchronous acquisition of the vibration and keyphasor signal (constant-time increment)

(2) Obtaining the speed of the shaft from the keyphasor signal and the total phase can be calculated

(3) Setting the resampling rate based on the maximum value of shaft speed, and then obtaining the even-angle increment and corresponding sampling time

(4) Interpolating the vibration signal according to the even-angle increment

2.3. Local Mean Decomposition. A series of product functions (PFs) can be obtained by the LMD processing method, and each PF is a monocomponent of the original signal [28]. The LMD method has been widely used to extract fault features for diagnosing rolling element bearing faults [29–31]. It can also be used as a signal denoising method by selecting an appropriate PF which contains the fault component signal. For a given signal $u(t)$, the LMD decomposition procedure consists of the following steps [32]:

Step 1. Extracting the extrema $z_i (i = 1, \ldots, M)$ of the original signal $u(t)$.

Step 2. Obtaining the local mean value m_i and the amplitude envelope estimate $a_i$from the two successive extrema.

$$\begin{aligned} m_i &= \frac{z_i + z_{i+1}}{2}, \quad i = 1, 2, \ldots, M-1, \\ a_i &= \frac{\left|z_i + z_{i+1}\right|}{2}, \quad i = 1, 2, \ldots, M-1. \end{aligned} \tag{4}$$

These local means are linked by straight lines with extending between successive extrema. The moving averaging can be done with averaging the right endpoint of each local mean with the left endpoint of the next local mean. The local mean function was repeatedly smoothed until there was no same value between two successive points. By this way, the continuous local mean function $m_{11}(t)$ is obtained. The continuous local magnitude envelope function $a_{11}(t)$ can be obtained by the same way [17].

Step 3. The continuous local mean function is subtracted from the original signal $u(t)$:

$$h_{11}(t) = u(t) - m_{11}(t), \tag{5}$$

The demodulated amplitude $s_{11}(t)$ is obtained with the envelope function $a_{11}(t)$:

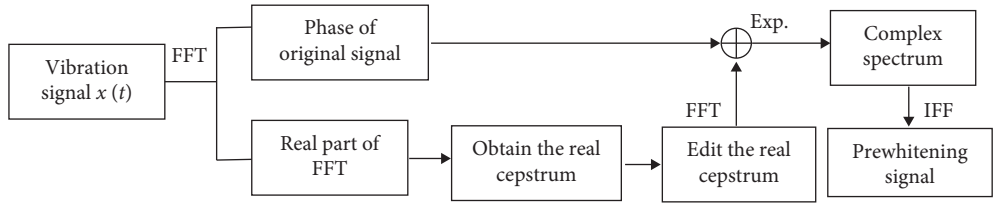

Figure 2: A flow chart of the cepstrum editing procedure.

$$s_{11}(t) = \frac{h_{11}(t)}{a_{11}(t)}. \tag{6}$$

Ideally, if $s_{11}(t)$ was a pure frequency modulated signal, its envelope function $a_{12}(t)$ should satisfy the conditions: $a_{12}(t) = 1$. If $a_{12}(t) \neq 1$, then $s_{11}(t)$ is taken as the new signal, and the mean values and amplitude envelope values are calculated by the extrema of $s_{11}(t)$. m_{12} and $a_{12}(t)$ are calculated by the same way of $m_{11}(t)$, and $a_{11}(t)\cdot s_{12}(t)$ also can be calculated via m_{12} and $a_{12}(t)$ based on equations (5) and (6). The process will stop until $s_{1n}(t)$ is the pure frequency modulated signal. The iteration is shown as follows:

$$\begin{cases} h_{11}(t) = x(t) - m_{11}(t), \\ h_{12}(t) = s_{11}(t) - m_{12}(t), \\ \quad \vdots \\ h_{1n}(t) = s_{1(n-1)}(t) - m_{1n}(t), \end{cases} \tag{7}$$

where $s_{1n}(t)$ is

$$\begin{cases} s_{11}(t) = \dfrac{h_{11}(t)}{a_{11}(t)}, \\ s_{12}(t) = \dfrac{h_{12}(t)}{a_{12}(t)}, \\ \quad \vdots \\ s_{1n}(t) = \dfrac{h_{1n}(t)}{a_{1n}(t)}. \end{cases} \tag{8}$$

Step 4. The envelop signal can be obtained as

$$a_1(t) = a_{11}(t)a_{12}(t)\cdots a_{1n}(t) = \prod_{p=1}^{n} a_{1p}(t), \quad \lim_{n \longrightarrow \infty} a_{1n}(t) = 1. \tag{9}$$

Thus, the envelope function $a_1(t)$ is expressed as the instantaneous amplitude. The instantaneous phase is

$$\theta_1(t) = \text{arc } cos\left(s_{1n}(t)\right). \tag{10}$$

The instantaneous frequency can be defined as

$$f_1(t) = \frac{1}{2\pi}\frac{d\theta_1(t)}{dt}. \tag{11}$$

Step 5. The first $\text{PF}_1(t)$ can be obtained from the product envelope function $a_1(t)$ and frequency modulated signal $s_{1n}(t)$:

$$\text{PF}_1(t) = a_1(t)s_{1n}(t). \tag{12}$$

Step 6. New data $u(t)$ can be obtained by subtracting $\text{PF}_1(t)$ from the original data. Then, steps 1–5 are repeated $k$times until $u_k(t)$ is a constant or does not contain oscillations. Finally, the original signal can be reconstructed:

$$x(t) = \sum_{p=1}^{k} \text{PF}_p(t) + u_k(t). \tag{13}$$

3. Continuous Wavelet Transform Analysis

The defect signature of a faulty bearing is similar to an impulse signal and is nonstationary. Energy is lost when the roller enters the leading edge of the defect area. The maximum energy is generated when the roller hits the ending edge of the defect area. Energy loss then occurs again when the roller departs the ending edge of defect area [6]. Considering this, the position of the entry and exit points can be identified with time-frequency analysis, which can represent the energy distribution of the vibration signal. To obtain a high resolution of the signal, the CWT is a suitable method. A scalogram can be obtained with the coefficients of the CWT. The coefficient matrix of CWT is defined as

$$W_c(a,b) = \int_{-\infty}^{+\infty} x(t)\overline{\psi}_{a,b}(t)\,dt, \tag{14}$$

where $x(t)$ is the signal, a is the scale, b is the translation, and $\psi_{a,b}(t)$is the mother wavelet:

$$\psi_{a,b}(t) = \frac{1}{\sqrt{a}}\psi\left(\frac{t-b}{a}\right). \tag{15}$$

It is very important to select a proper mother wavelet function for wavelet analysis. The Morlet wavelet is selected as the mother wavelet to analyze the signal because the shape of the wavelet is similar to the impulse component. The function of the Morlet wavelet is defined as

$$\psi(x) = \frac{1}{\sqrt{f_b\pi}} e^{-\left(x^2/f_b\right)} e^{j2\pi f_c x}. \tag{16}$$

Its Fourier transform is

$$\Phi(f) = e^{-\pi^2 f_b\left(f-f_c\right)^2}, \tag{17}$$

where f_b is the bandwidth parameter and f_c is the center frequency.

Equations (16) and (17) show that the time-frequency resolution of the wavelet depends on the bandwidth f_b and center frequency f_c [21]. The bandwidth parameter controls the oscillation attenuation of the Morlet wavelet. A larger f_b value results in a better frequency resolution, at the cost of a

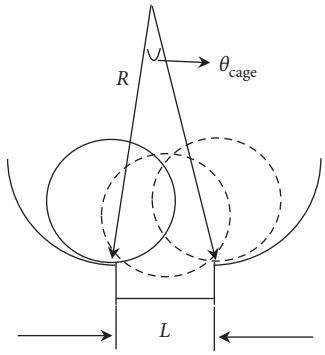

Figure 3: Model of roller passing over a defect.

lower time resolution. The larger the central frequency f_c is, the faster the Morlet wavelet will oscillate, which results in a lower frequency resolution. To obtain the best resolution, the parameters need to be optimized.

Shannon wavelet entropy is a good indicator for measuring sparsity. Jiang et al. [21] proposed an optimal method based on the modified Shannon wavelet entropy. The modified wavelet entropy is defined as

$$E_n(f_b) = -\sum_{i=1}^{M} p_i^k \log p_i^k,$$
$$\sum_{i=1}^{M} p_i^k = 1, \quad (18)$$
$$f_b \in [N, M],$$
$$f_c = k \in [A, B],$$

where p_i^k is calculated by

$$p_i^k(f_b) = \frac{\left|W_c^k(a_i, b)\right|}{\sum_{j=1}^{M}\left|W_c^k(a_j, b)\right|}. \quad (19)$$

Thus, the parameters of Morlet wavelet can be optimized in separate steps. An initial bandwidth $f_b \in [N, M]$ and center frequency $f_c \in [A, B]$ are chosen. To set the initial center frequency, a large initial bandwidth value is chosen. The Shannon entropy is then calculated by increasing the center frequency from A to B. The initial center frequency can be set based on the minimum wavelet entropy. Then, the bandwidth is increased from N to M, and the wavelet entropy $E_n(f_b)$ is calculated based on the initial center frequency. The optimized f_{ob} is selected based on the corresponding minimum wavelet entropy. By calculating the wavelet entropy by increasing the center frequency f_c from A to $B$with f_{ob}, the optimal f_c value is obtained based on the corresponding minimum wavelet entropy.

4. Fault Size Estimation

Once the entry and exit points were identified based on the Morlet wavelet analysis, the shaft's angular distance when roller passes over the defect area can be obtained. From Figure 3, the defect size can be calculated with angular duration as follows:

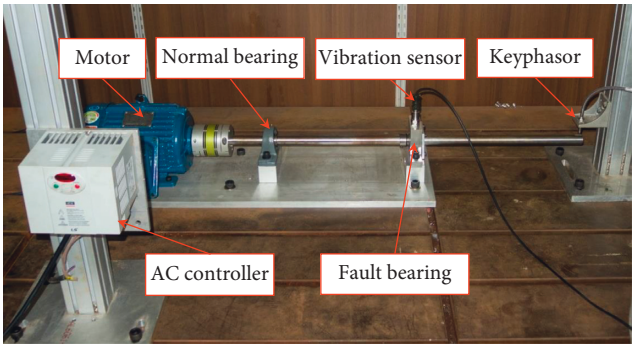

Figure 4: Rolling bearing test rig.

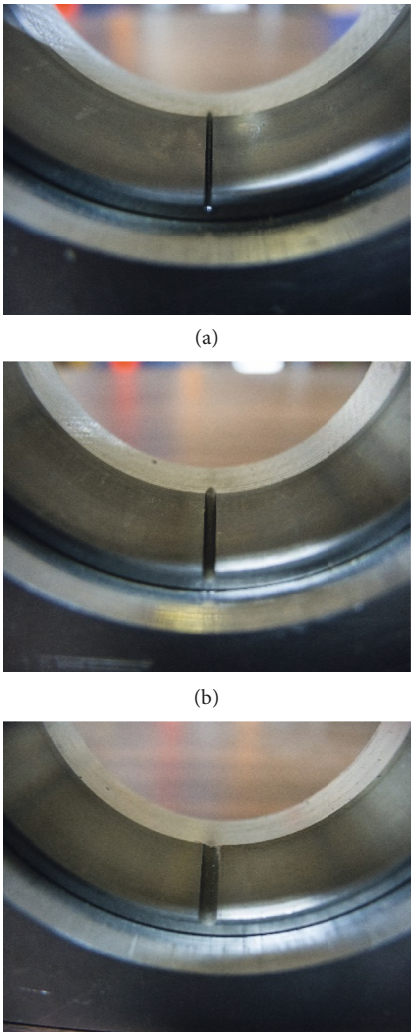

(a)

(b)

(c)

Figure 5: Different fault sizes on the outer races.

Table 1: Geometrical parameters of the test bearing.

Parameter	Value
Number of rolling elements (N_b)	17
Contact angle (α)	14°02′10
Ball diameter (d_{ball})	8.2 mm
Pitch diameter (D_p)	45.6 mm
Outer race inner radius (R)	27.05 mm

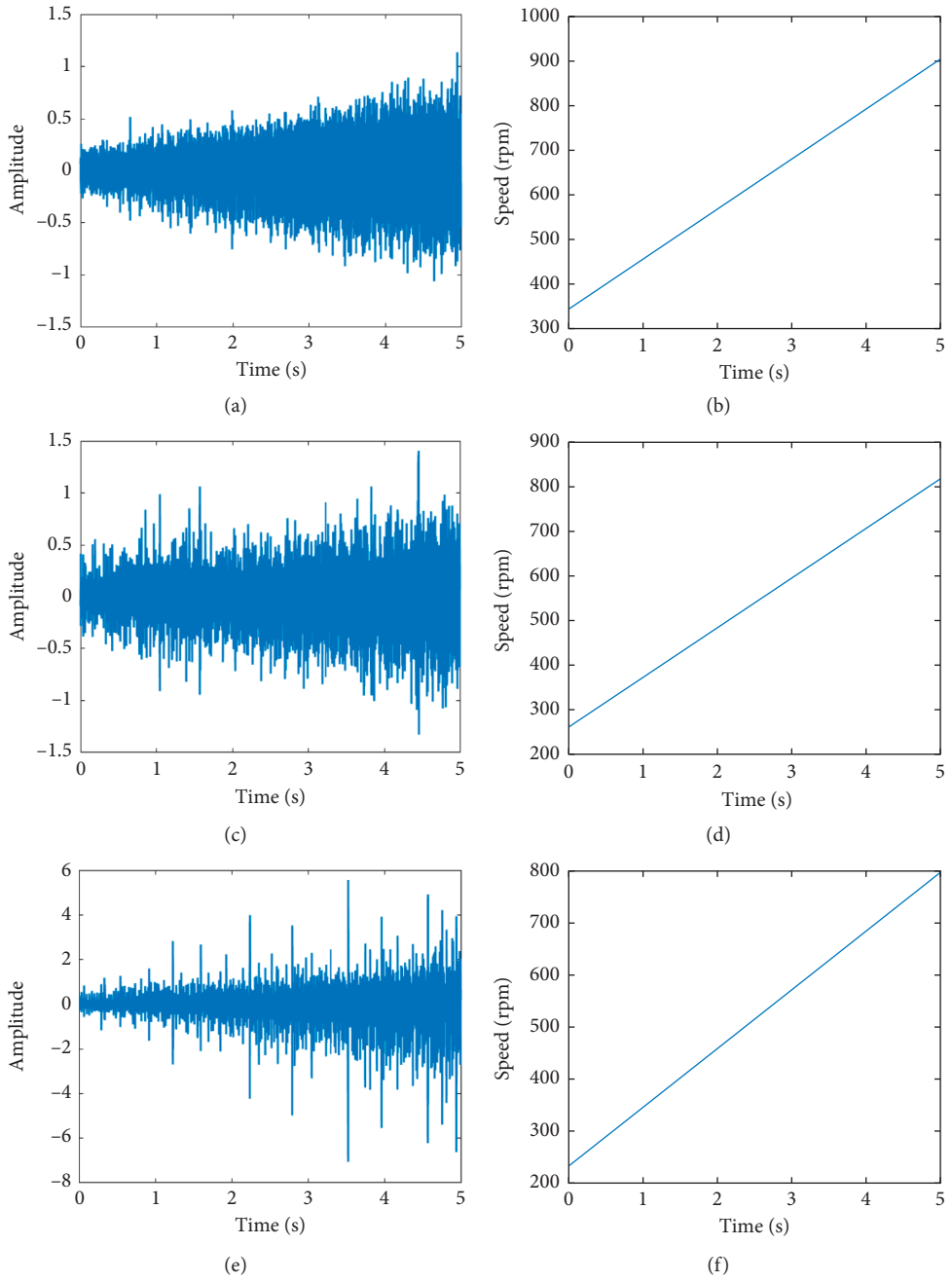

FIGURE 6: Vibration and speed signal of a bearing with different fault sizes on the outer race: (a), (c), (e) original vibration signal; (b), (d), (f) original speed signal.

$$L = R \times \theta_{\text{cage}},$$
$$L = R \times \theta_{\text{shaft}} \times \frac{f_{\text{cage}}}{f_{\text{shaft}}}, \tag{20}$$

where R is the outer race's inner radius, L is the defect width, and θ_{cage} and θ_{shaft} are the angular distances of the cage element and the shaft, respectively, when a roller passes over the defect area. f_{cage} and f_{shaft} are the cage and shaft speeds, respectively.

The relation between f_{cage} and f_{shaft} is as follows:

$$f_{\text{cage}} = \frac{f_{\text{shaft}}}{2} \times \left(1 - \frac{d}{D_{\text{p}}} \times \cos(\alpha)\right), \tag{21}$$

where d is the roller diameter, α is the contact angle, and D_{p} is the pitch diameter. This equation can be rewritten as

$$L = R \times \theta_{\text{shaft}} \times \frac{1}{2} \times \left(1 - \frac{d}{D_{\text{p}}} \times \cos(\alpha)\right). \tag{22}$$

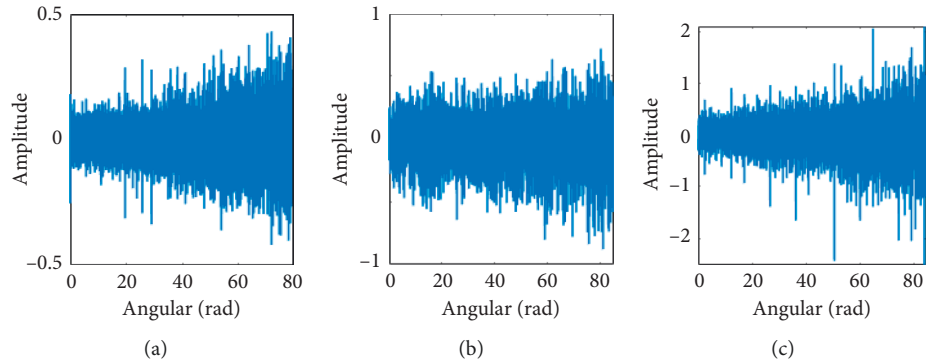

Figure 7: Prewhitening of vibration signal by edited cepstrum: (a) prewhitening signal of 0.75 mm defect size on the outer race. (b) Prewhitening signal of 1.5 mm defect size on the outer race. (c) Prewhitening signal of 2.5 mm defect size on the outer race.

Thus, once the angular distance is obtained, the fault size can be estimated.

5. Experiment Setup

Laboratory experiments were conducted with different fault defect sizes on the outer race to validate the proposed method. The experimental setup is shown in Figure 4. The test system consists of a 3-phase AC motor, a shaft supported by two rolling bearings, and an AC controller. The vibration signal is collected by an acceleration sensor that is mounted on the housing of the faulty bearing. The speed signal is collected by a tachometer mounted on the end of the shaft. All the data are obtained by an acquisition card (National Instrument) with a sampling frequency of 12000 Hz.

Three sets of rolling element bearings (NTN 30206) were used to estimate the defect size on the outer races. Three different defect sizes on the outer race (0.75, 1.5, and 2.5 mm) were made by electric discharge machining, as shown in Figure 5. The parameters of the rolling element bearing are listed in Table 1.

6. Results and Discussion

The original vibration signal and corresponding speed signal are shown in Figure 6. The amplitude of vibration signal increased as the shaft speed increased. The impact effect is more obvious when the defect size increases. The vibration signals were processed by the edited cepstrum to remove the determined component, and the results are shown in Figure 7. The amplitude of the prewhitened signal decreased after removing the determined component. However, the entry and exit points still could not be identified in the impulse component signal as random noise effect.

To estimate the defect size on the outer race, the time-domain signal needs to be resampled in the angular domain. Thus, the signal processed by the edited cepstrum method needs to be resampled in the angular domain before using the LMD method to extract the impact fault component.

During the resampling procedure, the signal is first upsampled by a factor of 10 to avoid aliasing. The resampled signal is obtained by recombining it with the speed signal, which was obtained from keyphasor data. The LMD decomposition result of the resampled signal with different fault sizes on outer race is shown in Figure 8. Several PFs can be obtained with the LMD process. The first PF is selected for further analysis because it has the biggest correlation coefficient value and keeps the most of information from original signal. By utilizing the LMD signal denoising method, the response of entry event and the impulse response of exit event were enhanced when rolling elements passed over the defect area on the outer race.

When using the continuous wavelet transform to process the denoised signal, the bandwidth and center frequency first need to be selected. The optimal parameters are selected based on the minimum Shannon wavelet entropy. The maximum order of this study is 400. The bandwidth is initialized as 400 to set the initial center frequency value. The initial bandwidth range is 1 to 30 with interval increment of 0.1, and the center frequency range is 0.1 to 5 with interval increment of 0.05. The initial center frequency and optimal parameters of each defect size are shown in Figures 9–11. Then, the signal was processed with CWT. At low speed (below 300 rpm), it is difficult to estimate the defect size due to the low signal energy and small response of the sensor in the low frequency range [7]. Thus, the defect size can be measured above 300 rpm.

To better demonstrate the processed result, a portion of the signal was selected to measure the defect size. Figures 12(a)–12(c) show the scalogram analysis results of the CWT with different defect widths on the outer race. To show the processed result more clearly, the details of the time-frequency analysis are shown in Figures 12(d) and 12(f). The impact response of the fault rolling bearing is like a sharp spike. Jena and Panigrahi [6] illustrated how to measure the defect width by using the CWT scalogram. The high energy zone is generated when a roller hits the end edge of the defect. The portion data are selected around this high energy zone. When a roller enters into the start edge of defect area, the energy decreased as the destressing effect. When a roller leaves the end edge of the

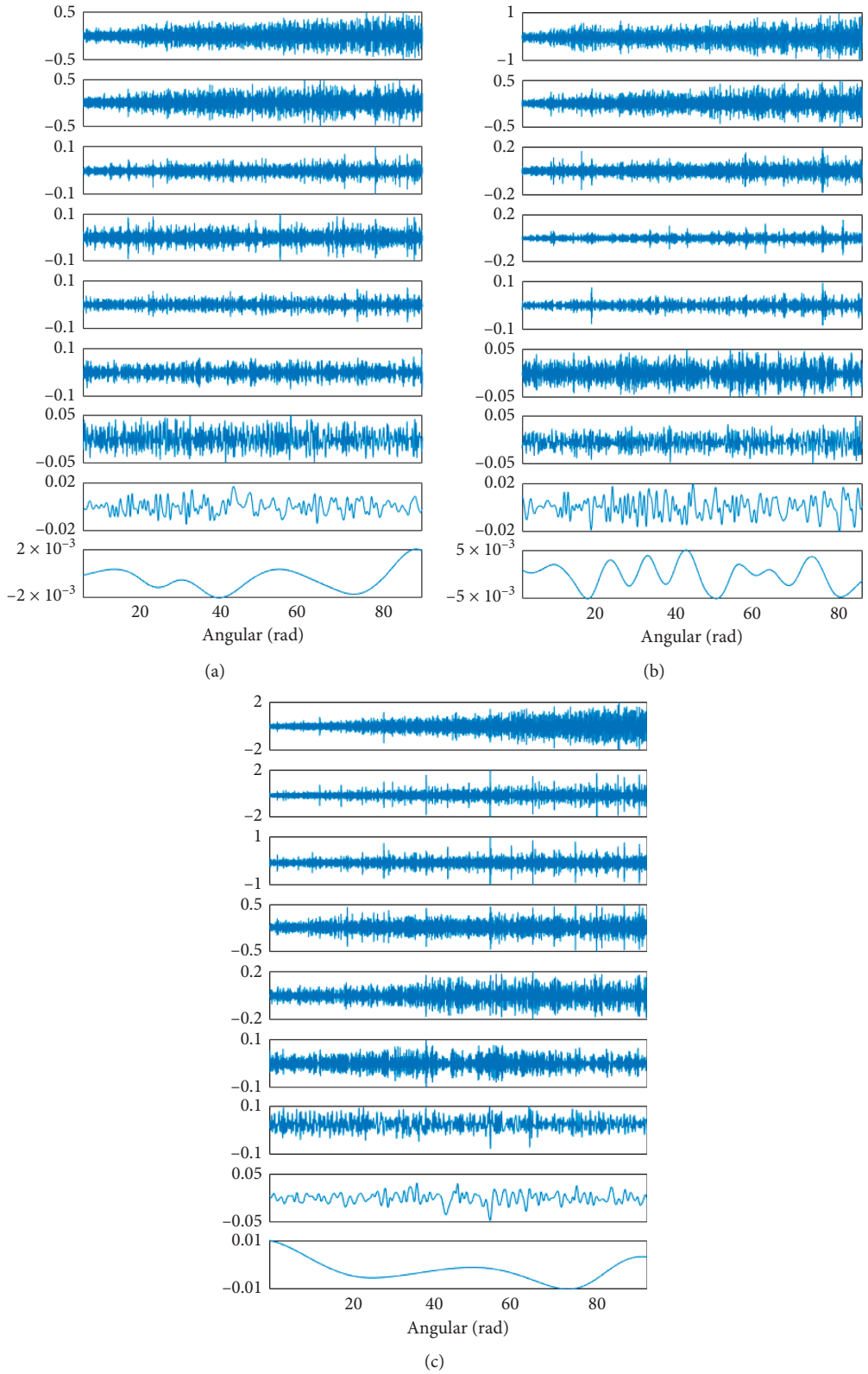

Figure 8: LMD decomposition result of resampled signal with different fault sizes on outer race: (a) 0.75 mm, (b) 1.5 mm, and (c) 2.5 mm.

defect, low energy zone was generated as the roller restresses back to its normal load condition. Thus, the entry point can be identified at the starting point of low energy zone (pre-side of high energy zone). The exit point can be identified at the end of low energy zone (postside of high energy zone). Once the entry and exit points are

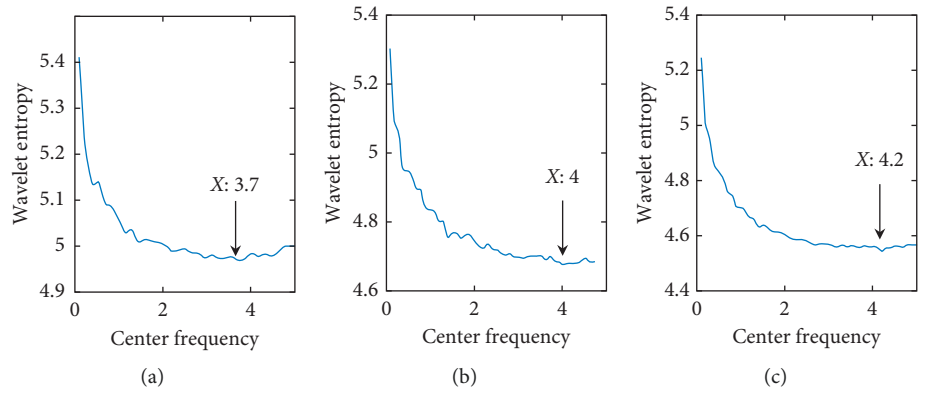

Figure 9: Relation between wavelet entropy and center frequency with a bandwidth of 400: (a) 0.75 mm, (b) 1.5 mm, and (c) 2.5 mm.

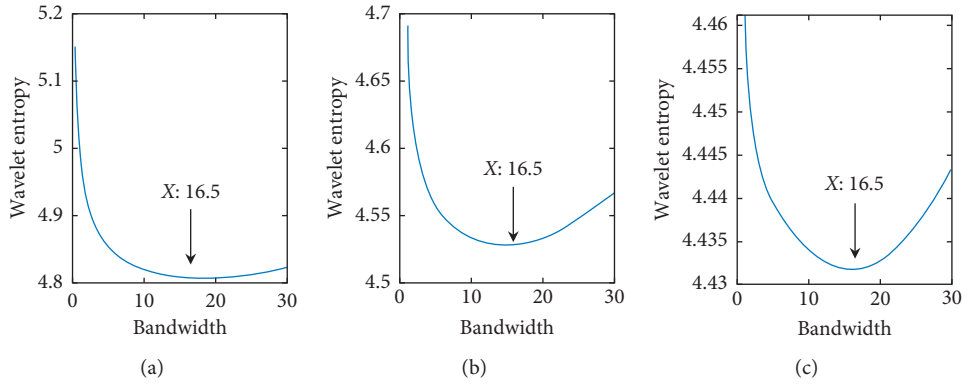

Figure 10: Relation between wavelet entropy and bandwidth parameters with the center frequency setting: (a) 0.75 mm, (b) 1.5 mm, and (c) 2.5 mm.

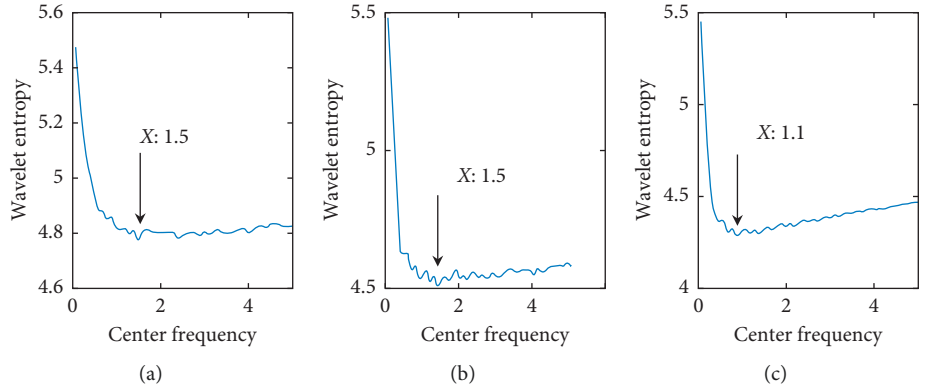

Figure 11: Relation between wavelet entropy and center frequency with optimal bandwidth: (a) 0.75 mm, (b) 1.5 mm, and (c) 2.5 mm.

identified, the angle duration was extracted, and the defect width can be measured.

The angle duration is estimated from the CWT scalogram for 10 portions of the signal that contain an impact component. The estimation result is shown in Table 2. The mean estimation value and deviation are obtained from the scalogram. The deviation values for the different defect sizes are 0.078, 0.066, and 0.05. The results show that the defect size on the outer race can be measured with the proposed method.

7. Conclusions

In this paper, a method was proposed to estimate the defect size on the outer race of a rolling bearing under time-varying speed conditions. To enhance the

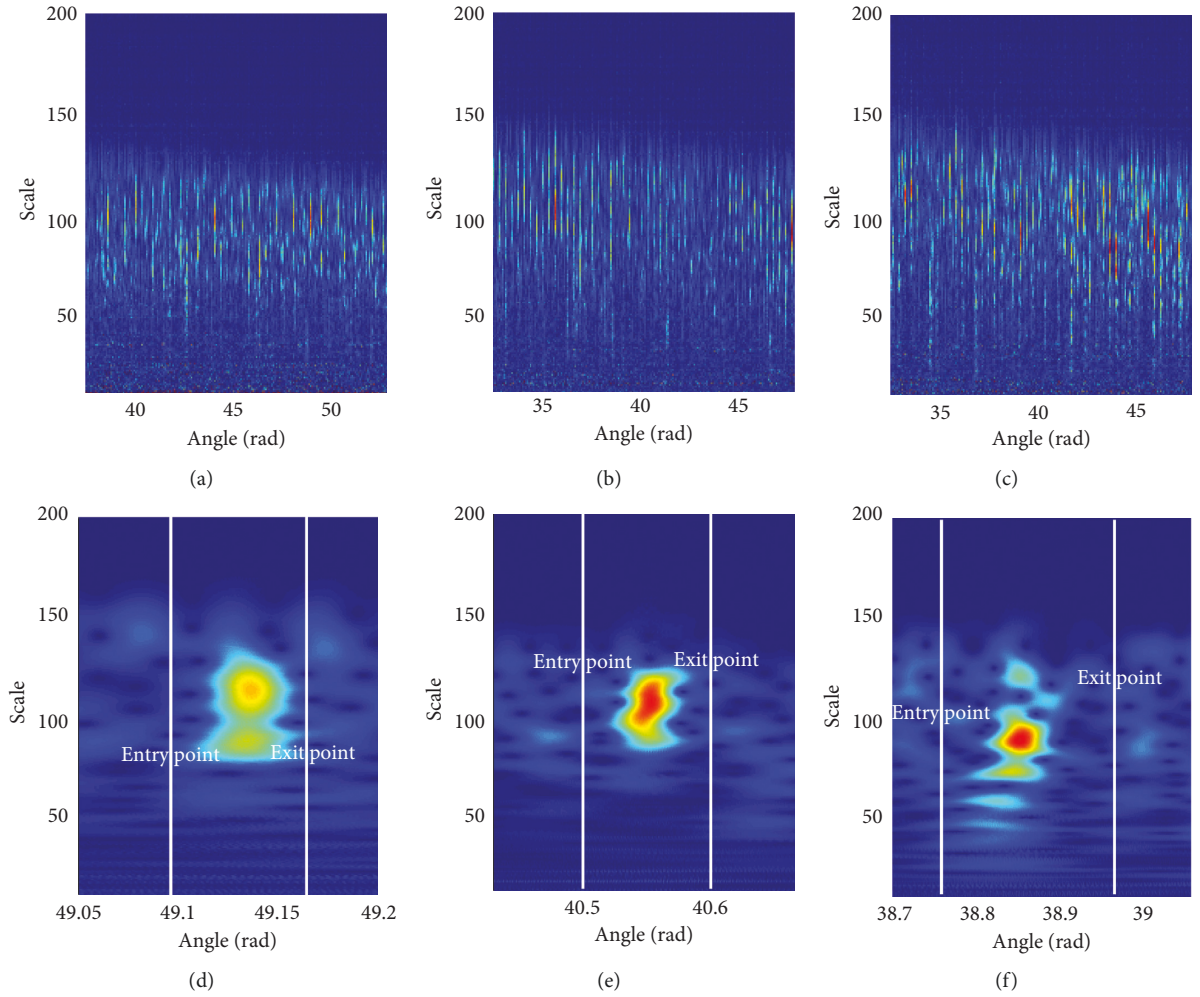

Figure 12: CWT analysis of the outer race fault: (a) CWT scalogram of 0.75 mm defect; (b) CWT scalogram of 1.5 mm defect; (c) CWT scalogram of 2.5 mm defect. (d–f) Detailed analysis of corresponding defect size.

Table 2: The estimation results of the defect size on the outer race.

Defects (mm)	Mean	Std. dev.
0.75	0.787	0.078
1.5	1.549	0.066
2.5	2.522	0.05

entry and exit events, the edited cepstrum was used to remove the determined components. To eliminate the speed variation effect and estimate the defect size, the edited signal was resampled with a constant angle interval. The LMD method was used to effectively extract the transient impulse component from the resampled signal. The CWT can provide full information about the energy distribution.

The entry and exit events of a roller passing over the defect on the outer race were identified clearly from the CWT spectrum. The average deviation of the estimated defect size was 6.5%. The estimation results show that the proposed method can effectively estimate the defect size on the outer race under time-varying speed conditions.

Data Availability

The vibration and keyphasor data used to support the findings of this study are available from the corresponding author upon request.

Conflicts of Interest

The authors declare that they have no conflicts of interest.

Acknowledgments

This work was supported by a 2017 grant from the Russian Science Foundation (Project no. 17-19-01389).

References

[1] M. Zhao, J. Lin, X. Xu, and Y. Lei, "Tacholess envelope order analysis and its application to fault detection of rolling element bearings with varying speeds," *Sensors*, vol. 13, no. 8, pp. 10856–10875, 2013.

[2] I. K. Epps, *An investigation into vibrations excited by discrete faults in rolling element bearings*, Ph.D. thesis, University of Canterbury Library, Christchurch, New Zealand, 1991.

[3] N. Sawalhi and R. B. Randall, "Vibration response of spalled rolling element bearings: observations, simulations and signal processing techniques to track the spall size," *Mechanical Systems and Signal Processing*, vol. 25, no. 3, pp. 846–870, 2011.

[4] N. Sawalhi, W. Wang, and A. Becker, "Vibration signal processing for spall size estimation in rolling element bearings using autoregressive inverse filtration combined with bearing signal synchronous averaging," *Advances in Mechanical Engineering*, vol. 9, no. 5, pp. 1–20, 2017.

[5] M. Ismail and N. Sawalhi, "Bearing spall size quantification based on geometric interpretation of vibration envelope energy," in *Proceedings of 13th International Conference on Condition Monitoring and Machinery Failure Prevention Technologies*, Paris, France, October 2016.

[6] D. P. Jena and S. N. Panigrahi, "Precise measurement of defect width in tapered roller bearing using vibration signal," *Measurement*, vol. 55, pp. 39–50, 2014.

[7] W. Moustafa, O. Cousinard, F. Bolaers, K. Sghir, and J. Dron, "Low speed bearings fault detection and size estimation using instantaneous angular speed," *Journal of Vibration and Control*, vol. 22, no. 15, pp. 3413–3425, 2014.

[8] S. Khanam, N. Tandon, and J. K. Dutt, "Fault size estimation in the outer race of ball bearing using discrete wavelet transform of the vibration signal," *Procedia Technology*, vol. 14, pp. 12–19, 2014.

[9] W. Wang, N. Sawalhi, and A. Becker, "Size estimation for naturally occurring bearing faults using synchronous averaging of vibration signals," *Journal of Vibration and Acoustics*, vol. 138, no. 5, article 051015, 2016.

[10] A. B. Ming, W. Zhang, Z. Y. Qin, and F. L. Chu, "Fault feature extraction and enhancement of rolling element bearing in varying speed condition," *Mechanical Systems and Signal Processing*, vol. 76-77, pp. 367–379, 2016.

[11] D. Zhao, J. Li, and W. Cheng, "Feature extraction of faulty rolling element bearing under variable rotational speed and gear interferences conditions," *Shock and Vibration*, vol. 2015, Article ID 425989, 9 pages, 2015.

[12] P. Borghesani, P. Pennacchi, S. Chatterton, and R. Ricci, "The velocity synchronous discrete Fourier transform for order tracking in the field of rotating machinery," *Mechanical Systems and Signal Processing*, vol. 44, no. 1-2, pp. 118–133, 2014.

[13] K. R. Fyfe and E. D. S. Munck, "Analysis of computed order tracking," *Mechanical Systems and Signal Processing*, vol. 11, no. 2, pp. 187–205, 1997.

[14] M.-C. Pan and Y.-F. Lin, "Further exploration of Vold-Kalman-filtering order tracking with shaft-speed information-I: theoretical part, numerical implementation and parameter investigations," *Mechanical Systems and Signal Processing*, vol. 20, no. 5, pp. 1134–1154, 2006.

[15] M.-C. Pan and Y.-F. Lin, "Further exploration of Vold-Kalman-filtering order tracking with shaft-speed information-II: engineering applications," *Mechanical Systems and Signal Processing*, vol. 20, no. 6, pp. 1410–1428, 2006.

[16] Y. Wang, G. Xu, Q. Zhang, D. Liu, and K. Jiang, "Rotating speed isolation and its application to rolling element bearing fault diagnosis under large speed variation conditions," *Journal of Sound and Vibration*, vol. 348, pp. 381–396, 2015.

[17] J. S. Smith, "The local mean decomposition and its application to EEG perception data," *Journal of the Royal Society Interface*, vol. 2, no. 5, pp. 443–454, 2005.

[18] L. Wang, Z. Liu, Q. Miao, and X. Zhang, "Time-frequency analysis based on ensemble local mean decomposition and fast kurtogram for rotating machinery fault diagnosis," *Mechanical Systems and Signal Processing*, vol. 103, pp. 60–75, 2018.

[19] H. Liu, W. Huang, S. Wang, and Z. Zhu, "Adaptive spectral kurtosis filtering based on Morlet wavelet and its application for signal transients detection," *Signal Processing*, vol. 96, pp. 118–124, 2014.

[20] W. Su, F. Wang, H. Zhu, Z. Zhang, and Z. Guo, "Rolling element bearing faults diagnosis based on optimal Morlet wavelet filter and autocorrelation enhancement," *Mechanical systems and signal processing*, vol. 24, no. 5, pp. 1458–1472, 2010.

[21] Y. Jiang, B. Tang, Y. Qin, and W. Liu, "Feature extraction method of wind turbine based on adaptive Morlet wavelet and SVD," *Renewable Energy*, vol. 36, no. 8, pp. 2146–2153, 2011.

[22] Y. Cao, M. Liu, J. Yang, Y. Cao, and W. Fu, "A method for extracting weak impact signal in NPP based on adaptive Morlet wavelet transform and kurtosis," *Progress in Nuclear Energy*, vol. 105, pp. 211–220, 2018.

[23] P. He, P. Li, and H. Sun, "Feature extraction of acoustic signals based on complex Morlet wavelet," *Procedia Engineering*, vol. 15, pp. 464–468, 2011.

[24] C. Peeters, P. Guillaume, and J. Helsen, "A comparison of cepstral editing methods as signal pre-processing techniques for vibration-based bearing fault detection," *Mechanical Systems and Signal Processing*, vol. 91, pp. 354–381, 2017.

[25] P. Borghesani, P. Pennacchi, R. B. Randall, N. Sawalhi, and R. Ricci, "Application of cepstrum pre-whitening for the diagnosis of bearing faults under variable speed conditions," *Mechanical Systems and Signal Processing*, vol. 36, no. 2, pp. 370–384, 2013.

[26] Y. Guo, T.-W. Liu, J. Na, and R.-F. Fung, "Envelope order tracking for fault detection in rolling element bearings," *Journal of Sound and Vibration*, vol. 331, no. 25, pp. 5644–5654, 2012.

[27] K. S. Wang, D. Guo, and P. S. Heyns, "The application of order tracking for vibration analysis of a varying speed rotor with a propagating transverse crack," *Engineering Failure Analysis*, vol. 21, pp. 91–101, 2012.

[28] H. Liu and M. Han, "A fault diagnosis method based on local mean decomposition and multi-scale entropy for roller bearings," *Mechanism and Machine Theory*, vol. 75, pp. 67–78, 2014.

[29] Y. Tian, J. Ma, C. Lu, and Z. Wang, "Rolling bearing fault diagnosis under variable conditions using LMD-SVD and extreme learning machine," *Mechanism and Machine Theory*, vol. 90, pp. 175–186, 2015.

[30] M. Han and J. Pan, "A fault diagnosis method combined with LMD, sample entropy and energy ratio for roller bearings," *Measurement*, vol. 76, pp. 7–19, 2015.

[31] W. Guo, L. Huang, C. Chen, H. Zou, and Z. Liu, "Elimination of end effects in local mean decomposition using spectral coherence and applications for rotating machinery," *Digital Signal Processing*, vol. 55, pp. 52–63, 2016.

[32] J. Cheng, Y. Yang, and Y. Yang, "A rotating machinery fault diagnosis method based on local mean decomposition," *Digital Signal Processing*, vol. 22, no. 2, pp. 356–366, 2012.